Quantum Electronics **48** (6) 537–544 (2018)

https://doi.org/10.1070/QEL16575

Subwavelength diffraction gratings in the visible spectral range

N.I. Petrov, V.A. Danilov, V.V. Popov, B.A. Usievich

Abstract. **We report the results of computer calculations and measurements of subwavelength diffraction gratings in the visible range of the radiation spectrum. The influence of various grating parameters (duty cycle, microrelief shape and depth, material, angle of incidence, wavelength, and radiation polarisation) on the diffraction efficiency is studied. A distinctive feature of the subwavelength gratings in question is that the entire diffracted energy of the beam is redistributed into the zero and –1st orders. It is found that the zero order can be suppressed by choosing the depth and shape of the grating relief. The subwavelength gratings with a period of 400 nm are fabricated and measurements are performed using lasers and laser diodes emitting in the visible wavelength range. High diffraction efficiency into the –1st order (more than 70%) is observed in a wide spectral range of 450–650 nm with an increase in the grating relief depth (at a depth of h = 80 nm). It is experimentally demonstrated that under certain conditions, the plasmon resonance effect arises, in which total absorption of incident radiation takes place. The optical elements considered can be used in image processing systems, projection displays, in the development of various sensors, etc.**

Keywords: *subwavelength grating, diffraction efficiency, plasmon resonance.*

1. Introduction

Interest in subwavelength gratings (with a grating period shorter than the emission wavelength) grows due to their promising applications in the high-efficient filters intended for the transmission and reflection of radiation [1], optoelectronic devices using surface plasmons [2–5], and spectrally selective external optical mirrors for vertical cavity surface emitting lasers (VCSELs) [6–8]. Wang et al. [9] proposed subwavelength gratings for the implementation of optical time delays without the use of waveguides of various lengths. Subwavelength gratings have been also proposed for light focusing both in the far [10] and near [11] zones.

Subwavelength dielectric gratings represent an alternative to distributed Bragg multilayer dielectric reflectors in the broadband highly reflecting devices for radiation filtration. Such structures are compact, inexpensive in manufacturing, and provide new possibilities for controlling the polarisation properties of radiation. Diffraction gratings also find application in the devices for splitting a light beam into colour components [12–18]. A new type of thin-film devices for separation of colours, based on the effect of frustrated total internal reflection, was considered in [19]. Such optical elements can be used for image processing in imaging systems, projection displays, etc. Petrov et al. [20] proposed and demonstrated subwavelength gratings for combining red, green, and blue light beams into a single common beam. It was shown that such gratings possess a high efficiency and can significantly reduce the size of projection devices used in mobile phones, etc. The efficiency of these devices is affected by a number of factors that depend on the material properties and grating structural parameters (including period, duty cycle, and microrelief depth).

Of practical interest are plasmonic metal-dielectric absorbing structures for frequency-selective and broadband absorbers. Such structures for radiation absorption in the far-IR spectral region were considered in [21].

This work shows that the total absorption effect can be observed in a metal subwavelength grating for visible radiation as well. The paper presents the results of computer calculations and measurements of subwavelength diffraction gratings.

2. Results of calculations

The theory of radiation diffraction on gratings has now been developed quite fully (see, for example, [22]). Since the scalar diffraction theory cannot be applied to subwavelength gratings [23], in this case the electromagnetic theory [24] based on the C-method [25–27] is used for calculations, the method applicability being mainly determined by the ratio of the grating microrelief depth to its period. The C-method makes it possible to obtain reliable results when the grating depth is less than its period [24]. The rigorous coupled-wave analysys (RCWA) for metal gratings faces the convergence problem in case of p-polarised radiation.

2.1. Diffraction efficiency

The diffraction efficiency of a grating is affected by a number of factors: duty cycle, microrelief shape and depth, grating material, angle of incidence, wavelength, and polarisation. Figure 1 shows the intensity distributions over the zero and –1st diffraction orders as a function of the radiation wavelength at different microrelief depths for the incident (a, c)

N.I. Petrov, V.A. Danilov Scientific and Technological Center of Unique Instrumentation, Russian Academy of Sciences, ul. Butlerova 15, 117342 Moscow, Russia; e-mail: petrovni@mail.ru;
V.V. Popov M.V. Lomonosov Moscow State University, Vorob'evy gory, 119991 Moscow, Russia;
B.A. Usievich A.M. Prokhorov General Physics Institute, Russian Academy of Sciences, ul. Vavilova 38, 119991 Moscow, Russia

Received 15 November 2017; revision received 1 February 2018
Kvantovaya Elektronika **48** (6) 537–544 (2018)
Translated by M.A. Monastyrskiy

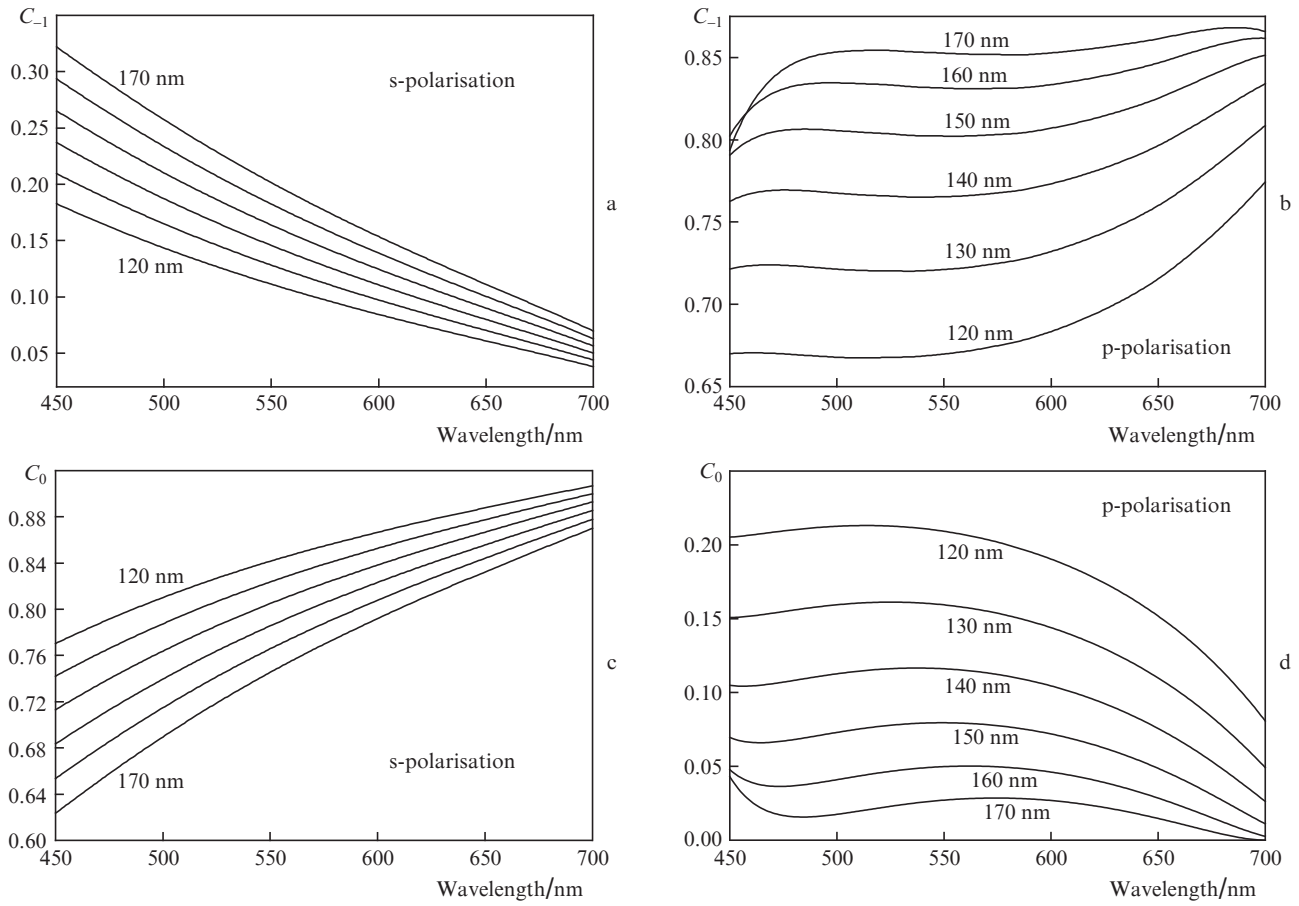

Figure 1. Diffraction efficiencies C_0 and C_{-1} as functions of the wavelength of (a, c) s-polarised and (b, d) p-polarised radiation for various microrelief depths of the aluminium grating with an isosceles triangle profile. The angle of incidence is $\theta_i = 60°$, and the grating period is $\Lambda = 400$ nm.

s-polarised and (b, d) p-polarised radiation, respectively. The angle of radiation incidence onto the grating is 60°. The profile of the grating grooves in the form of an isosceles triangle is considered. The triangle height (microrelief depth) varies from 120 to 170 nm with a step of 10 nm. The grating period is 400 nm, and the material is aluminium. It is seen that the diffraction efficiency C_{-1} increases with increasing depth of the grating microrelief. It should be noted that the absorption losses in the grating material are less than 15% in the visible wavelength range of 450–700 nm.

The diffraction efficiency increases with increasing grating depth for both p- and s-polarisations of light; herewith, in contrast to s-polarisation, in the case of p-polarisation, a bulk of incident radiation transits into the –1st diffraction order. This property should be taken into account when developing various devices using subwavelength gratings.

Figure 2 shows the diffraction efficiency in different spectrum orders for an aluminium sinusoidal grating with a period $\Lambda = 600$ nm as a function of the wavelength of p-polarised radiation for different microrelief depths. The incidence angle of p-polarised radiation is 5°. It is seen that in this case (in contrast to the subwavelength grating) a significant fraction of energy diffracts into the +1st order (Fig. 2c). It follows from the calculations that under certain conditions (radiation wavelength, angle of incidence) almost 100% of incident radiation is absorbed. Thus, at a radiation wavelength of $\lambda = 555$ nm and a microrelief depth of $h = 50$ nm, virtually entire radiation energy is absorbed by the grating (Fig. 2d). This property can be used to form nonreflective metal surfaces for various applications.

Similar dependences have been obtained for a nickel grating. Note that the absorption losses in the case of the nickel grating are much greater than those for the aluminium grating. In addition, most of the incident energy in the nickel grating passes into the zero order.

Figure 3 shows the diffraction efficiency as a function of the radiation wavelength for the gratings of various materials. The angle of incidence of p-polarised radiation onto the grating is 60°. We consider the grating profile in the form of an isosceles triangle, whose height (microrelief depth) is 160 nm. The grating period is $\Lambda = 400$ nm. The materials are aluminium, chrome, silver, gold, copper, and molybdenum. The material constants of substances were taken from [28–30]. As follows from the calculations, the change in diffraction efficiency is stronger for wavelengths in the blue region of the spectrum. It can be seen that the greatest diffraction efficiencies are attained when using silver and aluminium gratings.

The effect of the grating duty cycle on the diffraction efficiency is also studied. The duty cycle is defined as the inverse of the filling factor. The filling factor F specifies part of the grating period filled with the grating material. Thus, the equality $F = 0.5$ means that 50% of a cross section within the grating period is filled with metal, while the rest part – with air. We have considered the gratings with sinusoidal, triangular and trapezoidal profiles. Figure 4 shows the calculated dependences of the diffraction efficiency C_{-1} on the

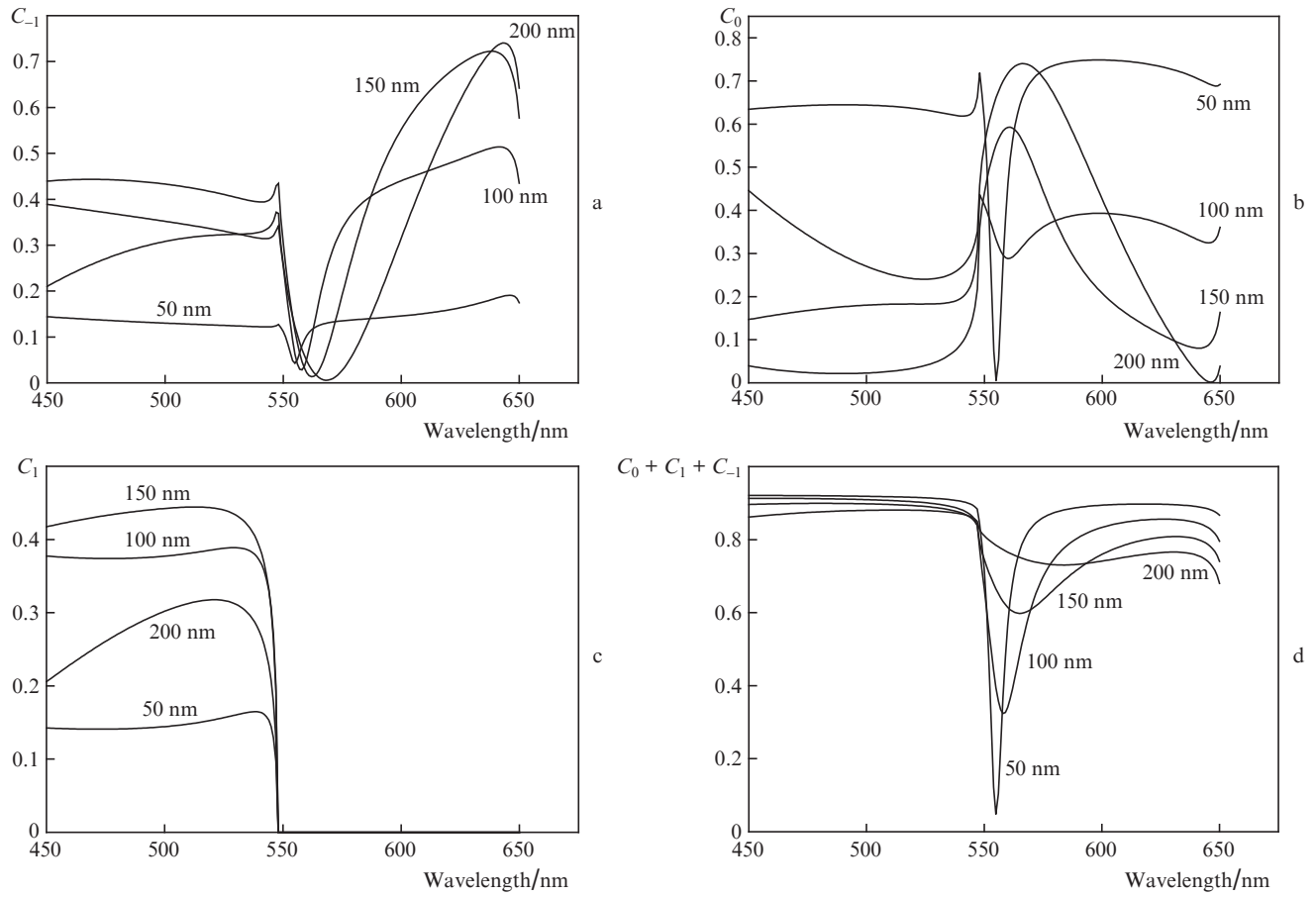

Figure 2. Diffraction efficiencies in different orders for an aluminium sinusoidal grating with a period $\Lambda = 600$ nm as a function of the wavelength of p-polarised radiation at different microrelief depths.

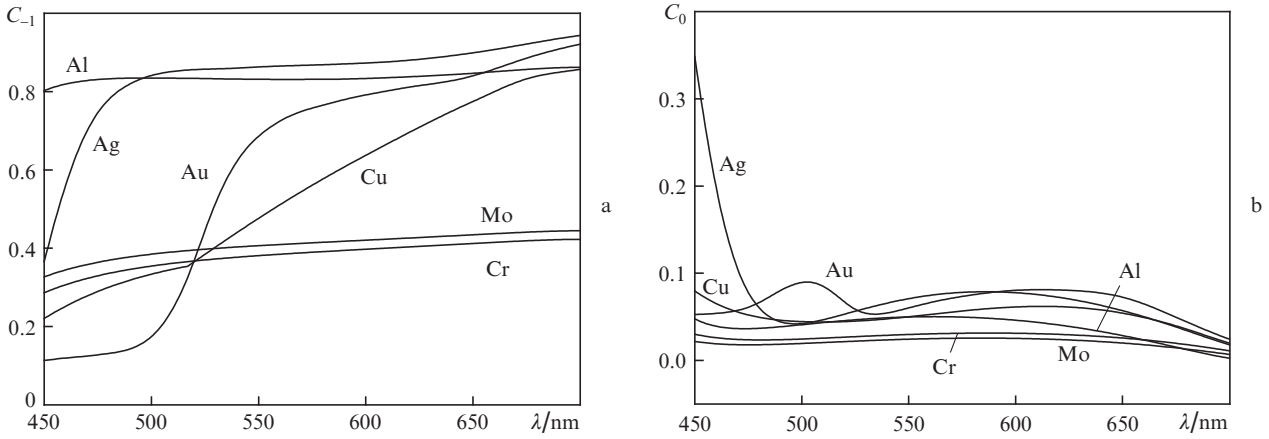

Figure 3. Diffraction efficiencies of the gratings from various materials as functions of the wavelength of p-polarised radiation.

radiation wavelength for sinusoidal and trapezoidal gratings made of aluminium. The following parameters of the grating and p-polarised incident radiation were used in the calculations: the grating period is $\Lambda = 400$ nm, the angle of incidence is $\theta_i = 60°$, and the grating height is $h = 160$ nm. It is seen that the diffraction efficiency is higher for a sinusoidal grating. It has been found that, in contrast to the case $\Lambda > \lambda$, the diffraction efficiencies of subwavelength gratings with different profiles are close to each other.

Figure 5 demonstrates the intensity distributions by diffraction orders as a function of the radiation wavelength for different values of the filling factor F for a trapezoidal aluminium grating. The angle of incidence onto the grating of the p-polarised radiation is 60°, the microrelief depth is 160 nm, and the grating period is 400 nm. As follows from the calculations, in the case of a trapezoidal grating, an increase in diffraction efficiency for the green and red regions of the spectrum is possible with decreasing F, though in this case

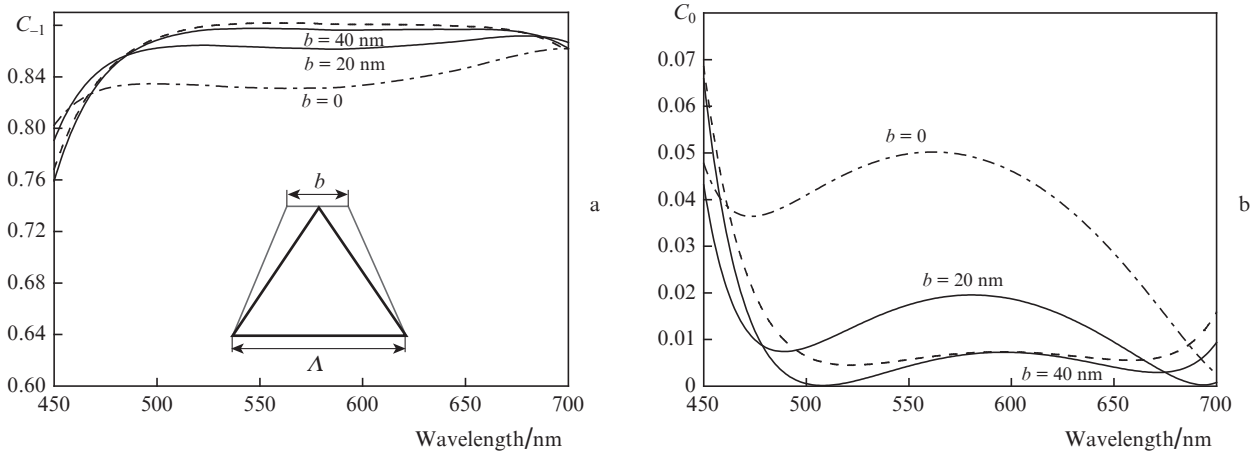

Figure 4. Diffraction efficiencies as functions of the wavelength of p-polarised radiation for aluminium gratings with (dashed curves) sinusoidal, (dash-dotted curves) triangular, and (solid curves) trapezoidal profiles; $\theta_i = 60°$, $\Lambda = 400$ nm, $h = 160$ nm. The inset shows the grating profile.

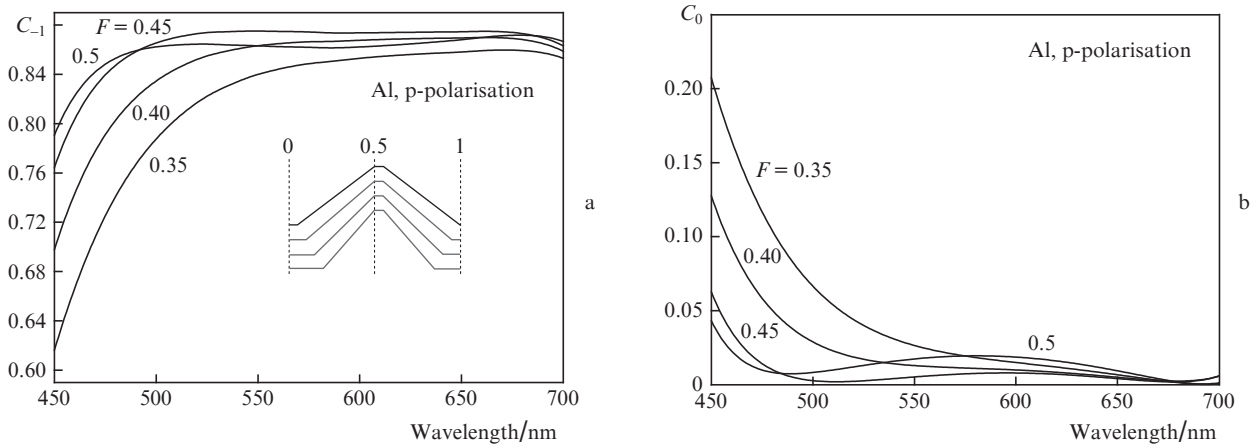

Figure 5. Intensity distributions over the diffraction orders as functions of the radiation wavelength at different filling factors F for a trapezoidal aluminium grating ($h = 160$ nm, $\Lambda = 400$ nm). The inset shows the grating profiles for various F.

the blue region efficiency is markedly reduced. It is seen that the influence of the grating profile shape is much stronger for the blue radiation.

Consider now a reflective diffraction grating for combining red (R), green (G) and blue (B) laser beams into a single common beam (Fig. 6). The angles of incidence for the light beams can be determined from the diffraction grating equation

$$\sin\theta_i + \sin\theta_w = \frac{m\lambda_i}{\Lambda}, \qquad (1)$$

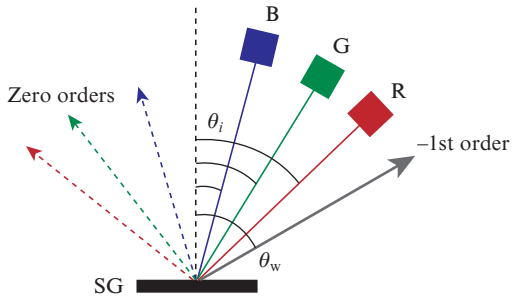

Figure 6. Subwavelength reflective grating (SG) combining the beams of red (R), green (G), and blue (B) lasers.

where θ_i are the angles of incidence for red, green, and blue light beams (i = R, G, B); θ_w is the angle of reflection of the combined light beam; λ_i are the wavelengths of red, green and blue light beams; and $m = \pm1, \pm2, \pm3, \ldots$ is the diffraction order.

From Eqn (1) we have the expression:

$$\theta_i = \arcsin\left(\frac{m\lambda_i}{\Lambda} - \sin\theta_w\right). \qquad (2)$$

To combine the beams of different colours, it is more efficient to use the –1st ($m = -1$) diffraction order to avoid mixing of the reflected white light beam with zero diffraction orders of the incident laser beams of different colours:

$$\theta_i = \arcsin\left(-\frac{\lambda_i}{\Lambda} - \sin\theta_w\right). \qquad (3)$$

It follows from (3) that at the angles of incidence $\theta_i = -49.4°$, $-27.6°$, and $-15°$ (for red, green, and blue beams, respectively), the angle of the beam diffracted into the –1st order (θ_w) constitutes $-60°$ for the grating period $\Lambda = 400$ nm. Note that in this case the +1st order is absent in the air and, accord-

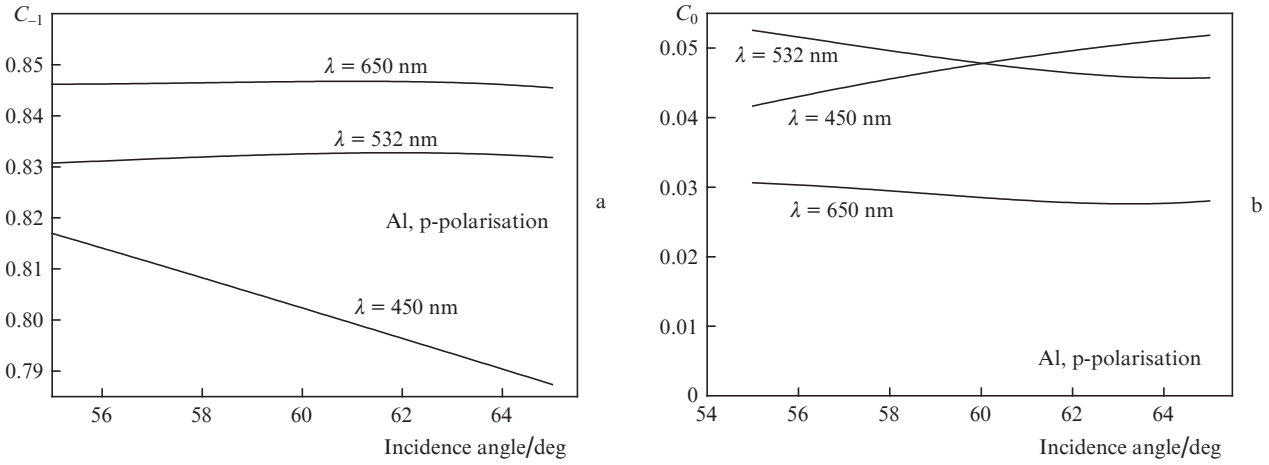

Figure 7. Diffraction efficiencies as a function of the angle of incidence of p-polarised radiation onto the aluminium grating with a relief profile in the shape of an isosceles triangle (h = 160 nm, Λ = 400 nm) for the radiation wavelengths of 450, 532, and 650 nm.

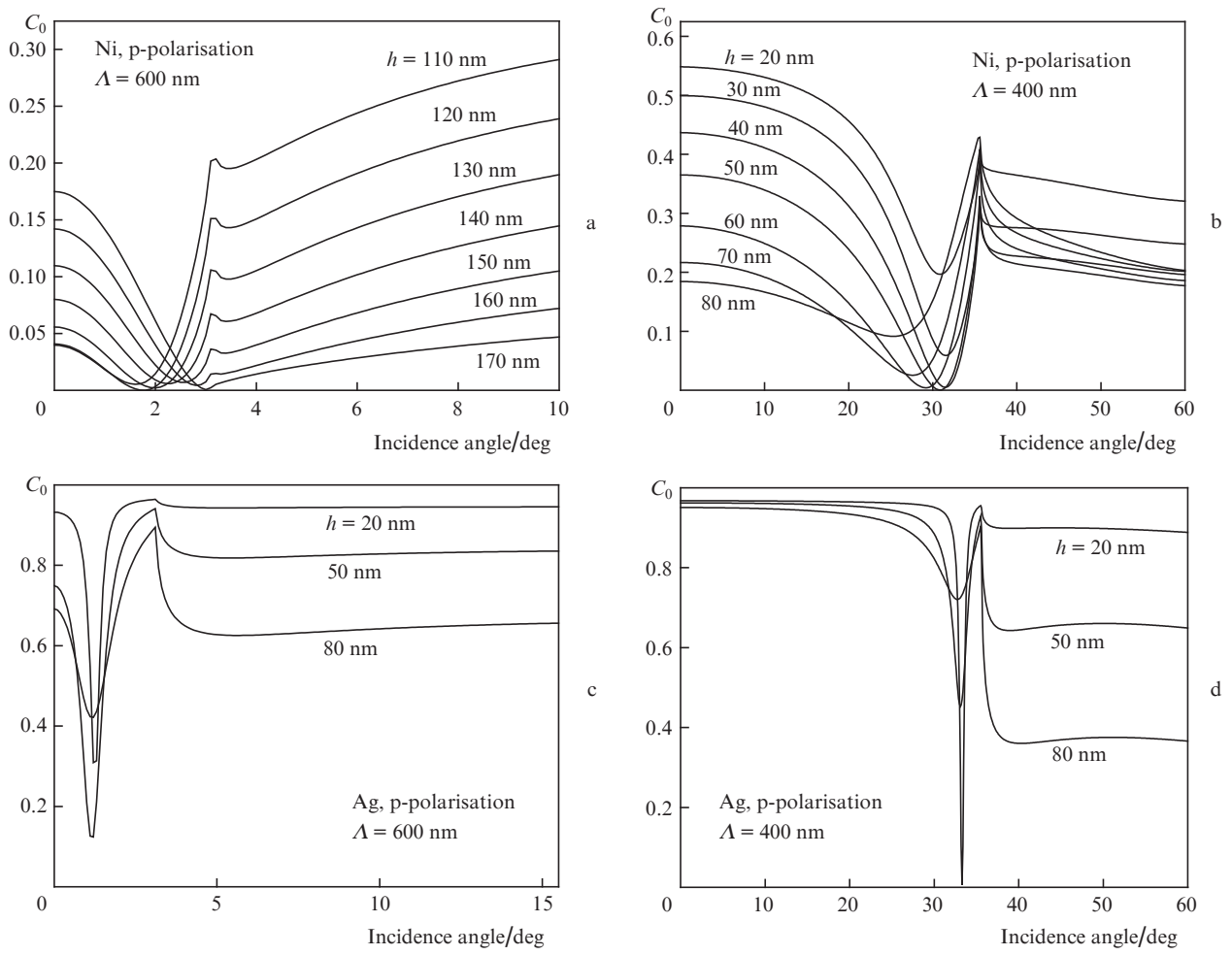

Figure 8. Diffraction efficiencies C_0 in the zero order as a function of the angle of incidence for different microrelief depths h of (a, b) nickel and (c, d) silver gratings at a wavelength of 641 nm, and a period Λ = (a, c) 600 and (b, d) 400 nm.

ingly, part of the power does not pass into this order, which has a positive effect on the diffraction efficiency in the working –1st order. For an aluminium grating with a microrelief depth of 160 nm, the efficiency values in the –1st order constitute 80%–85% for incident radiation in the wavelength range of 450–650 nm (Fig. 7).

2.2. Surface plasmons

Surface plasmons are excited by light with the aid of grating [31]. The excitation of surface plasmons in the case of noncollinear scattering by a metal diffraction grating was investigated in [3]. It is established in [4] that the resonance singularities in

the spectral angular dependences of the nanograting transmittance are stipulated by the excitation of surface metal–air and metal–dielectric plasmons.

If the grating constant is Λ, then the wave vector of light acquires the additive $2\pi/\Lambda$, and the dispersion relation for surface plasmons must take into account the wave vector component parallel to the surface. For the angle of incidence θ_i, the resonance condition takes the form

$$\frac{\omega}{c}\sin\theta_0 + \frac{2m\pi}{\Lambda} = \frac{\omega}{c}\sqrt{\frac{\varepsilon_r}{\varepsilon_r + 1}}, \quad (4)$$

where ε_r is the real part of dielectric permittivity of the grating material; and ω and c are the frequency and the speed of light.

We should note that the microrelief depth is not included into Eqn (4), and for deep gratings this equation can be considered only as an estimate. However, the resonance angles obtained from this equation are in good agreement with accurate calculations. By using (4), we can determine the angles of the radiation incidence onto the grating, at which the plasmon resonance arises. Table 1 gives the values of the angles of incidence of red, green, and blue beams for Al, Ni, and Ag gratings.

Figure 8 shows the diffraction efficiency in different orders for (a, b) nickel and (c, d) silver sinusoidal gratings with periods $\Lambda = 600$ nm and 400 nm as a function of the angle of incidence of p-polarised radiation with a wavelength $\lambda = 641$ nm at different microrelief depths h. At a certain angle of incidence, the effect of plasmon resonance is observed. It is seen that at a relief depth $h = 80$ nm and an incidence angle $\theta_i = 33°$, almost 100% of incident energy is absorbed by the silver grating (Fig. 8d). For the nickel grating, the complete absorption of incident radiation is attained at $h = 50$ nm and $\theta_i = 31°$ (Fig. 8b).

Table 1. Angles of incidence corresponding to the condition of plasmon resonance appearance ($\Lambda = 400$ nm) for various metals.

λ/nm	Angle of incidence θ_0/deg		
	Al	Ni	Ag
641	36.4	33.4	34.8
532	18.5	14.5	16.1
450	6.2	0.57	1.9

2.3. Diffraction in water and air

For the development of sensors, it is of interest to study diffraction in various media. Figure 9 shows the diffraction efficiency dependence of the nickel grating with a period of $\Lambda = 400$ nm on the incidence angle of p-polarised radiation with a wavelength of $\lambda = 632.8$ nm in water and air. It can be seen that the diffraction efficiencies into the –1st order are significantly different. If diffraction in water into the first order occurs at angles of incidence $\theta_i > 10°$, then in the air the –1st order of the diffracted beam only appears for $\theta_i > 35°$.

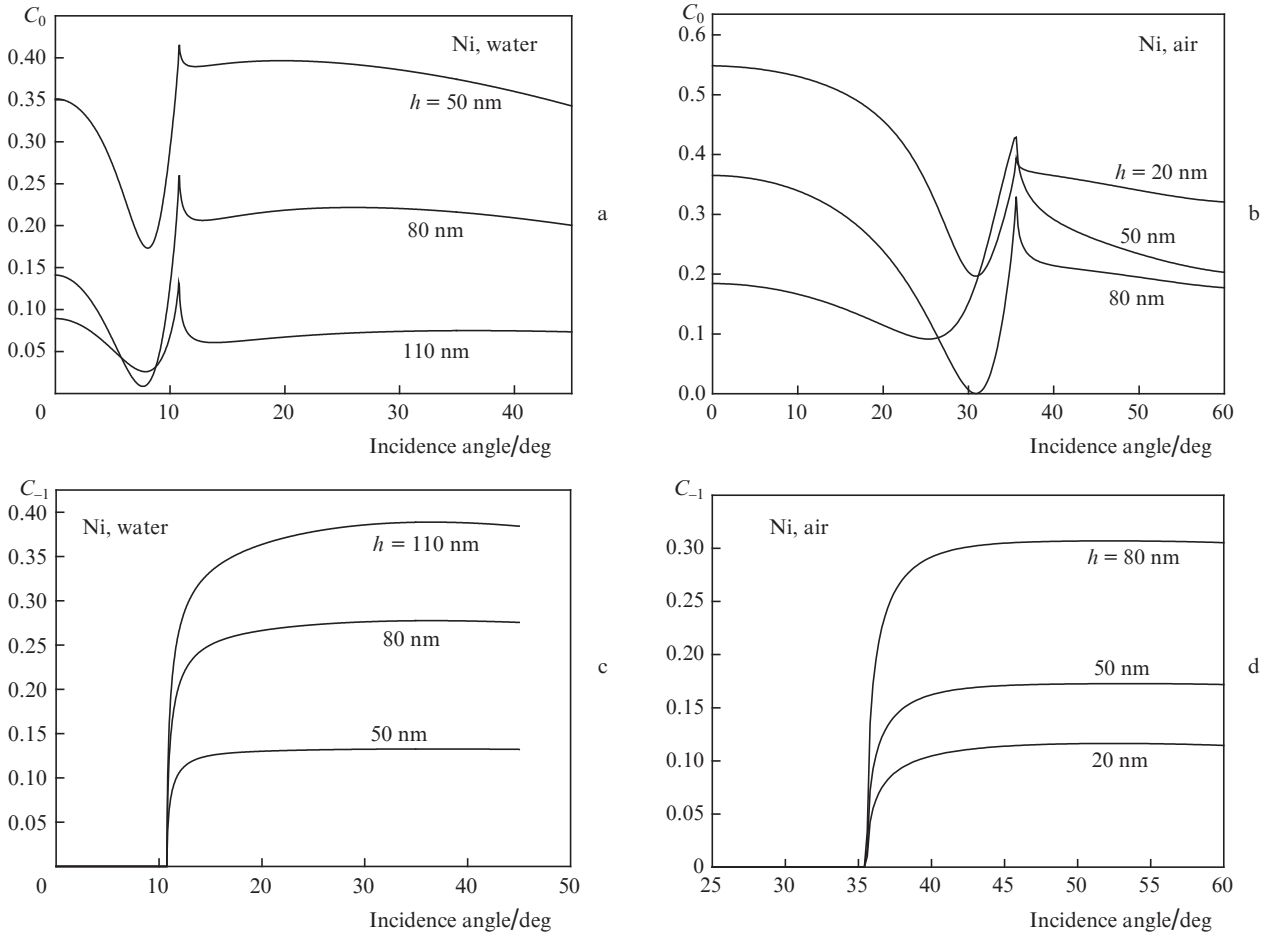

Figure 9. Diffraction efficiency as a function of the angle of radiation incidence in (a, c) water and (b, d) air for nickel gratings with various microrelief depths.

3. Measurements

Two groups of samples were investigated: original gratings and their nickel replicas. Original gratings were made using electron beam lithography [32] and etching in a polymethylmethacrylate (PMMC) film deposited on a chromatised glass substrate using spin-coating technology [33]. Figure 10 shows an image of a grating with a period of $\Lambda = 400$ nm, obtained with an atomic-force microscope (AFM). As follows from the AFM measurements, the shape of the grating profiles is well described by the trapezoidal model.

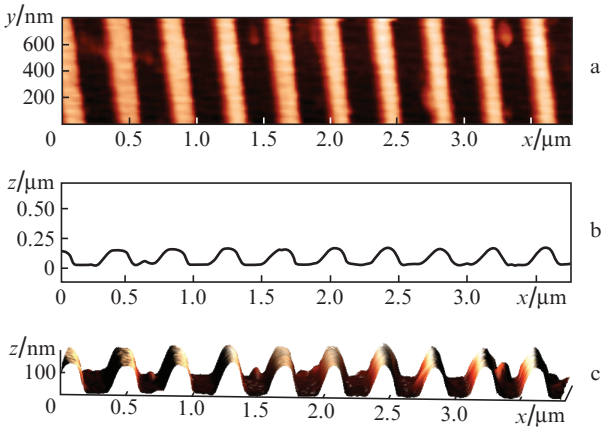

Figure 10. Images of gratings obtained with an NT-MDT Smena AFM: (a) top view, (b) side view, and (c) 3D image ($\Lambda = 400$ nm).

Using an optical power meter, the diffraction efficiency was measured as a function of the angle of incidence of light beams of red, green and blue colours (R, G, B), emitted by lasers and laser diodes with a power from 5 to 150 mW and diameters of beams from 1 to 3 mm. It should be noted that the metal grids possess stability to the radiation of sufficiently high power, while the sources used in the units for combining the beams in microprojection devices have a power of less than 2 mW.

Figure 11 shows the (points) measured and (solid curves) calculated diffraction efficiencies for red, green, and blue light beams as functions of the angle of incidence. Small discrepancies arise because of the imperfect grating profile and inaccuracy in measuring the grating height. At the incidence angles of 49.4°, 27.6°, and 15° for red, green, and blue beams, respectively, a 70% combining efficiency can be obtained for a grating with a microrelief depth of 80 nm. Higher efficiency can be attained for gratings with greater microrelief depths, made of a suitable material. The efficiency may exceed 85% when using a grating with a depth of $h = 170$ nm.

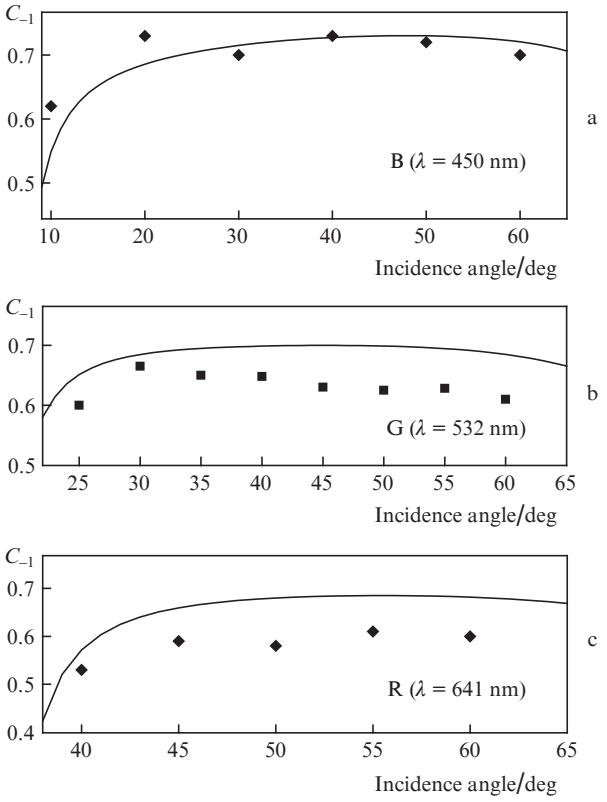

Figure 11. (Solid curves) Calculated and (points) measured diffraction efficiencies C_{-1} as functions of the light incidence angle for a silver grating with a period $\Lambda = 400$ nm and a rectangular profile depth $h = 80$ nm for (a) blue light with $\lambda = 450$ nm, (b) green light with $\lambda = 532$ nm, and (c) red light with $\lambda = 641$ nm.

Figure 12 presents the results of calculations and measurements of the diffraction efficiency into the zero order for a

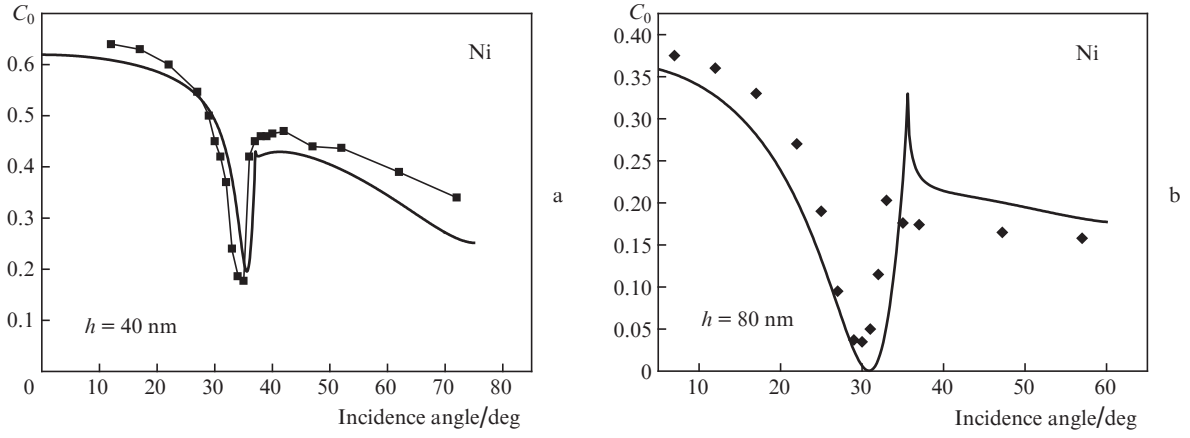

Figure 12. (Solid curves) Calculated and (points) measured diffraction efficiencies into the zero order as functions of the incidence angle of p-polarised radiation for a nickel grating with a period $\Lambda = 400$ nm, and a depth $h =$ (a) 40 and (b) 80 nm at the radiation wavelength $\lambda = 641$ nm.

nickel grating as a function of the angle of incidence for p-polarised radiation at different microrelief depths. It is seen that at an incidence angle of ~33°, the effect of plasmon resonance occurs. At the relief depth $h = 80$ nm and incidence angle $\theta_i = 31°$, almost entire energy is absorbed by the grating. Note that the measured angles of incidence at which the plasmon resonance effect occurs are in good agreement with the calculated ones.

4. Discussion and conclusions

It follows from the results of modelling and experiments that the diffraction efficiency is higher for p-polarised incident light beams. This means that the device combining the incident beams R, G and B should be designed to operate with p-polarisation. However, in this case, a phenomenon of surface plasmon resonance occurs, which reduces the device efficiency. These difficulties can be eliminated by choosing the appropriate angles of incidence or using a different material. Indeed, the plasmon resonance occurs in a narrow range of angles. The resonance appearance depends on the material permittivity, and thus this effect exists not for all metals.

A distinctive feature of subwavelength gratings is that the entire diffracted energy of a beam is redistributed into the zero and –1st orders. As is seen from Eqn (1), other orders also exist for ordinary gratings. The zero order can be suppressed by choosing the depth and shape of a grating. This makes it possible to obtain high efficiency in the –1st order for multicolour beams in a wide spectral range (450–650 nm) on the same grating.

For subwavelength gratings, the profile can be symmetrical, with a high diffraction efficiency being attained for both sinusoidal and trapezoidal profiles. It should be noted that the diffraction efficiency for the trapezoidal profile only slightly depends on the radiation wavelength; therefore such gratings are preferable for practical applications.

In plasmon resonance, it is possible to find the optimal parameters of a grating (material, microrelief depth) and of radiation (angle of incidence, polarisation) at which the reflected and diffracted light is completely absent; in other words, there is a 100% absorption of incident radiation energy by the metal subwavelength grating in the visible spectral range. This property can be used in the development of various devices, in particular, in solar panels and displays.

Thus, the conducted studies have shown that it is possible to obtain a high diffraction efficiency of a subwavelength grating in a wide spectral range (450–650 nm). Subwavelength gratings can be used in the development of sensors and pico-projectors, where the efficiency and compactness are the determining factors, and also for image processing in 3D displays, projection displays, etc. The results obtained can be useful in the development of new devices for combining [34] and/or separation of light beams and the devices based on the plasmon excitation effect [35, 36].

Acknowledgements. This work was supported by the Russian Science Foundation (Grant No. 17-19-01461).

References

1. Tibuleac T.S., Magnusson R. *J. Opt. Soc. Am. A*, **14**, 1617 (1997).
2. Ghaemi H.F., Thio T., Grupp D.E., Ebbesen T.W., Lezec H.J. *Phys. Rev. B*, **58**, 6779 (1998).
3. Andreev A.V., Korneev A.A., Mukina L.S., Nazarov M.M., Prudnikov I.R., Shkurinov A.P. *Quantum Electron*., **35**, 27 (2005) [*Kvantovaya Elektron*., **35**, 27 (2005)].
4. Andreev A.V., Grischenko Yu.V., Dobynde M.I., et al. *Pis'ma Zh. Eksp. Teor. Fiz*., **92**, 823 (2010).
5. Lee K.Y., Yoon J.W., Song S.H., Magnusson R. *Sci. Rep*., **7**, 46508 (2017).
6. Block S., Gamet E., Pigeon F. *IEEE J. Quantum Electron*., **41**, 1049 (2005).
7. Huang M.C.Y., Zhou Y., Chang-Hasnain C.J. *Nature Photon*., **1**, 119 (2007).
8. Czyszanowski T., Gebski M., Dems M., Wasiak M., Sarzała R., Panajotov K. *Sci. Rep*., **7**, 40348 (2017).
9. Wang J., Ashrafi R., Adams R., Glesk I., Gasulla I., Capmany J., Chen L.R. *Sci. Rep*., **6**, 30235 (2016).
10. Fattal D., Li J., Peng Z., Fiorentino M., Beausoleil R.G. *Nature Photon*., **4**, 466 (2010).
11. Cheng Y.C., Zeng H., Trull J., Cojocaru C., Malinauskas M., Jukna T., Wiersma D.S., Staliunas K. *Opt. Lett*., **39**, 6086 (2014).
12. Dammann H. *Appl. Opt*., **17**, 2273 (1978).
13. Farn M.W., Stern M.B., Veldkamp W.B., Medeiros S.S. *Opt. Lett*., **18**, 1214 (1993).
14. Liu Chun-Wei, Lee Chi-Hung, Yang Tzu-Chun, Ting Chia-Jen, Lin Tsung-Hsin, Lin Shih-Chieh. *Appl. Opt*., **52**, 3617 (2013).
15. Veldkamp W.B., Leger J.R., Swanson G.J. *Opt. Lett*., **11**, 303 (1986).
16. Cheung E.C., Ho J.G., Goodno G.D., Rice R.R., Rothenberg J., Thielen P., Weber M., Wickham M. *Opt. Lett*., **33**, 354 (2008).
17. Shiono T., Hamamoto T., Takahara K. *Appl. Opt*., **41**, 2390 (2002).
18. Destouches N., Tishchenko A.V., Pommier J.C., Reynaud S., Parriaux O., Tonchev S., Abdou A.M. *Opt. Express*, **13** (9), 3230 (2005).
19. Petrov N.I. *Opt. Lett*., **32**, 2744 (2007).
20. Petrov N.I., Nikitin V.G., Danilov V.A., Popov V.V., Usievich B.A. *Appl. Opt*., **53**, 5740 (2014).
21. Vial B., Demesy G., Zolla F., et al. *J. Opt. Soc. Am. B*, **31**, 1339 (2014).
22. http://www.fresnel.fr/files/gratings/Second-Edition/.
23. Gremaux D.A., Gallagher N.C. *Appl. Opt*., **32**, 1948 (1993).
24. http://www.mcgrating.com/.
25. Chandezon J., Maystre D., Raoult G. *J. Optics (Paris)*, **11**, 235 (1980).
26. Chandezon J., Dupuis M.T., Cornet G. *J. Opt. Soc. Am*., **72**, 839 (1982).
27. Li L. *J. Opt. Soc. Am*., **11**, 2816 (1994).
28. http://www.gsolver.com.
29. http://www.luxpop.com/#index%20of%20refraction%A0.
30. http://RefractiveIndex.info.
31. Raether H. *Surface Plasmons on Smooth and Rough Surface and on Gratings* (Berlin: Springer-Verlag, 1988).
32. Fujita T., Nishihara H., Koyama J. *Opt. Lett*., **7**, 578 (1982).
33. Novikova T., De Martino A., Bulkin P., Nguyen Q., Drevillon B., Popov V., Chumakov A. *Opt. Express*, **15**, 2033 (2007).
34. Chaoa Weichung, Chi Sien, Wu Ching Yi, Kuo Chung J. *Opt. Commun*., **151**, 21 (1998).
35. Sun Xiaoliang, Shu Xuewen, Chen Changhong. *Appl. Opt*., **54**, 1548 (2015).
36. Petrov N.I., Danilov V.A., Popov V.V., Usievich B.A. *Frontiers in Optics/Laser Science Conf. (FiO/LS)* (Washington, USA, 2017) Paper JW3A.107.